Mechanistic Regimes of Vibronic Transport in a Heterodimer and the Design Principle of Incoherent Vibronic Transport in Phycobiliproteins

Bennett, Doran I.G.; Malý, Pavel; Kreisbeck, Christoph; Van Grondelle, Rienk; Aspuru-Guzik, Alán

published in
Journal of Physical Chemistry Letters
2018

DOI (link to publisher)
10.1021/acs.jpclett.8b00844

document version
Publisher's PDF, also known as Version of record

THE JOURNAL OF PHYSICAL CHEMISTRY Letters

Cite This: J. Phys. Chem. Lett. 2018, 9, 2665−2670

Letter

pubs.acs.org/JPCL

Mechanistic Regimes of Vibronic Transport in a Heterodimer and the Design Principle of Incoherent Vibronic Transport in Phycobiliproteins

Doran I. G. Bennett,*[,†,‡] Pavel Malý,[§,∥,‡] Christoph Kreisbeck,[†] Rienk van Grondelle,[§,‡] and Alán Aspuru-Guzik[†,‡]

[†]Department of Chemistry and Chemical Biology, Harvard University, 12 Oxford Street, Cambridge, Massachusetts 02138, United States

[‡]Bio-Inspired Solar Energy Program, Canadian Institute for Advanced Research, Toronto, Ontario M5G 1Z8, Canada

[§]Department of Physics and Astronomy, Faculty of Sciences, VU University Amsterdam, De Boelelaan 1081, 1081 HV Amsterdam, The Netherlands

[∥]Institute of Physics, Faculty of Mathematics and Physics, Charles University, Ke Karlovu 3, 121 16 Prague 2, Czech Republic

Supporting Information

ABSTRACT: Following the observation of coherent oscillations in nonlinear spectra of photosynthetic pigment protein complexes, in particular, phycobilliproteins such as PC645, coherent vibronic transport has been suggested as a design principle for novel light-harvesting materials. Vibronic transport between energetically remote pigments is coherent when the presence of a vibration resonant with the electronic energy gap supports transient delocalization between the electronic excited states. We establish the mechanism of vibronic transport for a model heterodimer across a wide range of molecular parameter values. The resulting mechanistic map demonstrates that the molecular parameters of phycobiliproteins in fact support incoherent vibronic transport. This result points to an important design principle: Incoherent vibronic transport is more efficient than a coherent mechanism when energetic disorder exceeds the coupling between the donor and vibrationally excited acceptor states. Finally, our results suggest that the role of coherent vibronic transport in pigment protein complexes should be reevaluated.

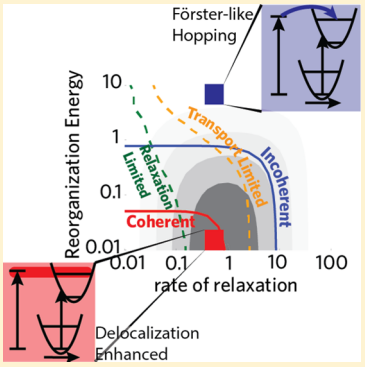

Excitation transport down an energy gradient, like that observed in some photosynthetic or artificial light-harvesting complexes, requires the dissipation of excess electronic energy into molecular vibrations. Vibronic transport is a photophysical process that converts an electronic excitation on one pigment to an electronic and vibrational excitation on another pigment (or vice versa). Vibronic transport between detuned pigments has been identified as a potential design principle for accelerating or controlling exciton migration in next-generation materials.[1−5] Realizing the advantages of engineered vibrational environments in practical devices, however, requires a clear understanding of how the mechanism of vibronic transport changes as a function of the chemical structure and vibrational dynamics of the pigments.

Vibronic transport between energetically remote pigments is coherent when the presence of a vibration resonant with the electronic energy gap supports transient delocalization between the pair of electronic excited states. Coherent transport allows for a ballistic spread (population width $\propto$ time^2) of an initially localized excitation that outraces the diffusive transport (population width $\propto$ time) supported by incoherent mechanisms.[6,7] Following the observation of coherent oscillations in nonlinear spectroscopy, many researchers have suggested that biological pigment protein complexes (PPCs) use coherent vibronic transport to enhance the rate of light harvesting,[3,8−11] but this remains controversial.[5,12−14] The continued controversy, despite numerically exact simulations of exciton transport in the presence of a resonant high-frequency vibration,[2,5,8,11,12,15] points to the need for a clear articulation of the relationship between molecular parameter values and the emergent mechanism of vibronic transport, similar to what was previously achieved for electronic transport mechanisms.[16−19] Here we will simulate a minimal vibronic heterodimer to establish how the vibronic transport mechanism varies across molecular parameter space. These results map out the mechanistic regimes and are appropriate for analyzing a wide variety of vibronic dimers. We use the mechanistic map to demonstrate that phycobiliproteins, a family of PPCs that remains a cannonical example of coherent vibronic transport thought to occur at room temperature,[1−3,20,21] in fact undergo incoherent vibronic transport. This result points to a basic design principle we suggest is important for understanding vibrationally mediated exciton transport in both natural and

Received: March 18, 2018
Accepted: April 23, 2018
Published: April 23, 2018

DOI: 10.1021/acs.jpclett.8b00844
J. Phys. Chem. Lett. 2018, 9, 2665−2670

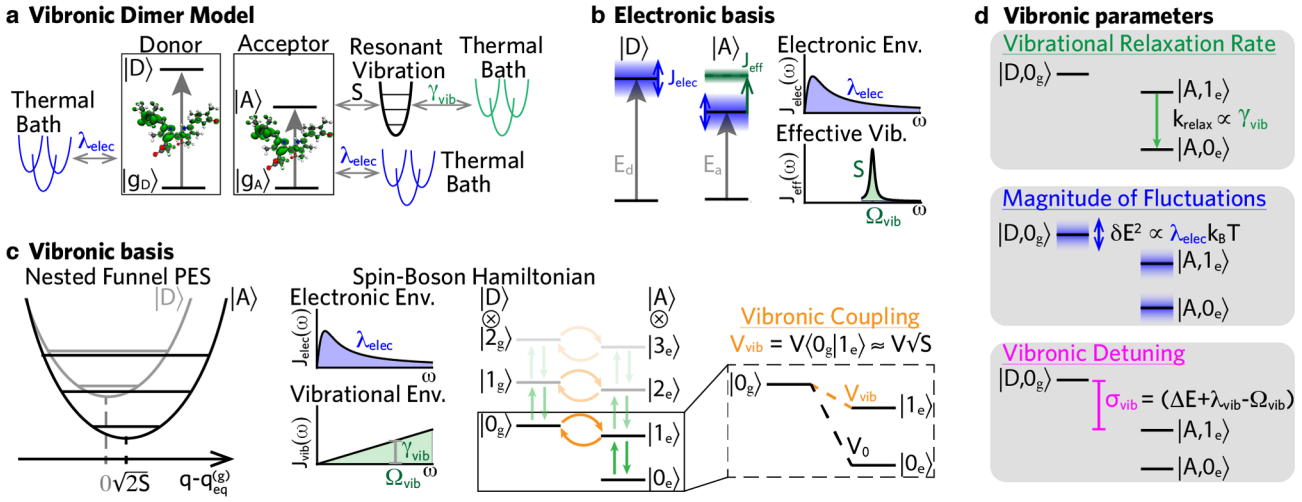

Figure 1. (a) Schematic representation of a vibronic dimer Hamiltonian. (b) Diagrammatic representation of the electronic states ($|A\rangle$,$|D\rangle$) and the corresponding spectral densities in the electronic basis. (c) "Nested Funnel PES": The system Hamiltonian expressed as potential energy surfaces (PES) when the high-frequency vibration is explicitly included. The donor PES (gray line, $|D\rangle$) is a vertically displaced copy of the ground-state PES. The acceptor PES (black line, $|A\rangle$) is both vertically and horizontally displaced from the ground state. The horizontal displacement of the equilibrium position is $\sqrt{2S}$. "Spin Boson Hamiltonian": The system Hamiltonian expressed in the vibronic basis and the corresponding spectral densities. "Vibronic Coupling": The coupling between the lowest energy donor and the vibrationally excited acceptor state (V_{vib}) is smaller than the electronic coupling between the lowest energy donor and lowest energy acceptor states ($V_0 = V\langle 0_g|0_e\rangle \approx V$). (d) Schematic representations of the parameters that determine the mechanism of vibronic transport. k_{relax} is the rate of vibrational relaxation, which is proportional to γ_{vib}. δE^2 is the variance of the vertical excitation energy of the pigments, which is proportional to λ_{elec}. σ_{vib} is the energy gap between the lowest energy donor and vibrationally excited acceptor state.

artificial materials: Incoherent vibronic transport is more efficient than a coherent mechanism when energetic disorder exceeds the coupling between the donor and vibrationally excited acceptor states. Finally, our results suggest that the role of coherent vibronic transport for nonbilin PPCs should also be reevaluated.

In the following, we use a spin-boson Hamiltonian (Figure 1a) to explore the mechanism of vibronic transport in a model heterodimer where the electronic excitation of the donor (E_d, $|D\rangle$) and acceptor (E_a, $|A\rangle$) pigments have an energy gap much larger than the electronic coupling ($\Delta E = E_d - E_a \gg V$). In this model, we make use of a linear response formalism[22−24] that allows for an exact coarse-graining of vibrational motion into collections of effective harmonic oscillators. The electronic states of both pigments are coupled to independent collections of low-frequency vibrations ("electronic environment", Figure 1b,c) that form a thermal bath described by an overdamped Brownian oscillator spectral density

$$J_{elec}(\omega) = 2\lambda_{elec}\frac{\omega\gamma_{elec}}{\omega^2 + \gamma_{elec}^2} \quad (1)$$

where λ_{elec} is the reorganization energy and γ_{elec} is the peak width. The low-frequency vibrations capture the inertial component of the vibrational response to pigment excitation that can arise, for example, from solvent librational modes.[24,25] All of the main text results use $\gamma_{elec} = 50\ cm^{-1}$, as often assumed for photosynthetic PPCs.[16] Most pigment excitations are also coupled to many high-frequency intramolecular vibrations, as studied using, for example, fluorescence line narrowing measurements[26] and ab initio simulations,[5,27,28] but here we incorporate only a single high-frequency vibration coupled to the acceptor that directly mediates donor-to-acceptor transport. The high-frequency vibration is, in turn, coupled to a continuum of vibrational modes that form a thermal bath and cause the relaxation of vibrational excitations. In the electronic basis (Figure 1b), we describe the combined influence of the high-frequency vibration and its thermal bath on the excitation energy of the pigments through an underdamped Brownian oscillator spectral density ("effective vibration", Figure 1b)

$$J_{eff}(\omega) = 2\lambda_{vib}\frac{2\gamma_{vib}\Omega_{vib}^2\omega}{(\Omega_{vib}^2 - \omega^2)^2 + 4\gamma_{vib}^2\omega^2} \quad (2)$$

where $\lambda_{vib} = S\cdot\Omega_{vib}$ is the reorganization energy, S is the Huang−Rhys factor, γ_{vib} is the peak width, and Ω_{vib} is the vibrational frequency. We note that in all calculations presented here there is a negligible rate of transport between the donor and acceptor in the absence of the high-frequency vibration, allowing us to focus on the vibronic transport mechanism.

Whereas simulations performed in the electronic basis can provide an exact description of the net excitation transport between the donor and acceptor, they cannot provide clear insight into the underlying vibronic mechanism because the dynamics of the resonant vibration are not explicitly described.

To illuminate the mechanism of vibronic transport, the high-frequency vibration can be included in the system Hamiltonian,[2,29−32] and the resulting potential energy surface (PES) can be described as a nested funnel,[32] shown in Figure 1c. Because the vibration is an intramolecular mode on the acceptor pigment, donor excitation results in an excited-state PES (Figure 1c) that is equivalent to the ground-state but vertically shifted by the excitation energy of the donor molecule (gray curve, vibrational states: $|\nu_g\rangle$); electronic excitation of the acceptor is coupled to the vibration, however, and results in an excited-state PES that is both vertically and horizontally displaced (black curve, vibrational states: $|\nu_e\rangle$). The system Hamiltonian can be recast in the basis of vibronic states (Spin-Boson Hamiltonian, Figure 1c), which are indexed by both the electronic state of the dimer and the nuclear quantum number of the explicit vibration ($|A,\nu_e\rangle$, $|D,\nu_g\rangle$). The coupling

DOI: 10.1021/acs.jpclett.8b00844
J. Phys. Chem. Lett. 2018, 9, 2665−2670

("vibronic coupling", Figure 1c) between the lowest-energy donor state ($|D,0_g\rangle$) and the vibrationally excited acceptor state ($|A,1_e\rangle$) is given by

$$V_{vib} = V\langle 0_g|1_e\rangle \approx V\sqrt{S} \tag{3}$$

where V is the bare electronic coupling and $\langle 0_g|1_e\rangle$ is the Franck-Condon factor. The energy gap (σ_{vib}) between these states ("Vibronic Detuning", Figure 1d) depends on the vertical excitation energy difference between the pigments (ΔE), the vibrational reorganization energy (λ_{vib}), and the vibrational frequency (Ω_{vib}).

In the vibronic basis there are still two thermal environments that must be considered. The low-frequency vibrations ("electronic environment", Figure 1c) are described by the same overdamped Brownian oscillator used in the electronic basis. This results in the pigment excitation energies fluctuating ("Magnitude of Fluctuations", Figure 1d) with a variance (δE^2) proportional to λ_{elec}. The thermal bath coupled to the high-frequency vibration is described by a second spectral density (J_{vib}) that drives transport between states that have the same electronic indices but vibrational quantum numbers that differ by ±1 (green arrows, Figure 1c). When the effective spectral density (J_{eff}, eq 2) capturing the combined influence of the high-frequency vibration and thermal bath in the electronic basis is described by an underdamped Brownian oscillator, the thermal bath of vibrational modes coupled to the resonant vibration ("vibrational environment", Figure 1c) is described by an Ohmic spectral density[22] (Supporting Information section IC)

$$J_{vib}(\omega) = \frac{\gamma_{vib}}{\Omega_{vib}}\omega e^{-\omega/\omega_c} \tag{4}$$

where ω_c is the cutoff frequency assumed to be much larger than the frequency of the resonant vibration ($\omega_c \gg \Omega_{vib}$). In this case, the rate of relaxation from the vibrationally excited acceptor state to the vibrational-ground state ("Vibrational Relaxation", Figure 1d) is proportional to γ_{vib}. We note that in the absence of this additional spectral density in the vibronic basis the high-frequency vibration of a resonant vibronic heterodimer does not thermalize, leading to an incorrect equilibrium distribution with equal donor and acceptor populations.

In what follows, we track the mechanism of vibronic transport across the space of vibronic parameters expressed in reduced units defined by their ratio to the vibronic coupling: $\Gamma_{vib} = \frac{\gamma_{vib}}{V_{vib}}$, $\Lambda_{elec} = \frac{\lambda_{elec}}{V_{vib}}$, $\Sigma_{vib} = \frac{\sigma_{vib}}{V_{vib}}$. We find that vibronic Redfield[31] reproduces exciton dynamics simulated with hierarchically coupled equations of motion (HEOM)[33,34] when the low-frequency vibrations are Markovian (Supporting Information section IIIB), as we assume here. Therefore, in the following we use HEOM simulations in the electronic basis, as implemented in *QMaster*,[35] to study the overall rate of transport between the donor and acceptor, and we use vibronic Redfield simulations to characterize the underlying vibronic mechanism. Computational details are given in Supporting Information section II. We will begin by considering the case where the donor and vibrationally excited acceptor states have the same energy ($\Sigma_{vib} = 0$), and, therefore, vibronic transport is a resonant process. This represents the best-case scenario for coherent vibronic transport. In reality, of course, molecular complexes experience a disordered ensemble of configurations with a distribution of energy gaps between the donor and vibrationally excited acceptor states; we will return at the end to consider how disorder influences optimal behavior in photosynthetic pigment protein complexes and engineered devices.

The defining feature of coherent vibronic transport in a heterodimer is transient delocalization between the donor and the vibrationally excited acceptor states, which has been hypothesized to enhance the overall rate of transport between the detuned donor and acceptor pigments ($k_{a\leftarrow d}$) compared with an incoherent vibronic hopping mechanism. Figure 2a shows a contour plot of $k_{a\leftarrow d}$ when the donor and vibrationally excited acceptor state are in resonance ($\Sigma_{vib} = 0$) as a function of the magnitude of thermal fluctuations (Λ_{elec}) and the rate of relaxation (Γ_{vib}). Here we determine $k_{a\leftarrow d}$ by a one-exponential fit to the total acceptor population (summed over all vibrational states) simulated with HEOM (Supporting Information section

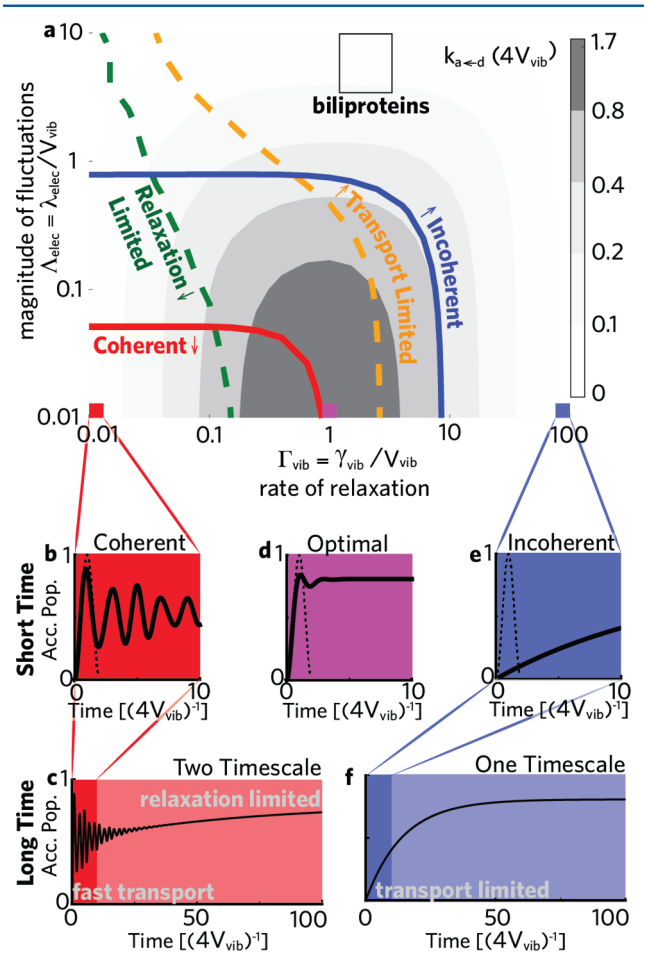

Figure 2. (a) Overall rate from the donor to acceptor is plotted as a function of the magnitude of thermal fluctuations (Λ_{elec}) and the rate of relaxation (Γ_{vib}) when the donor and vibrationally excited acceptor states are in resonance ($\Sigma_{vib} = 0$). Mechanistic regimes are bounded by colored lines. To the left (right) of the red (blue) solid line is the coherent (incoherent) regime. To the left (right) of the green (orange) dashed line, dynamics are relaxation (transport)-limited. The phycobiliprotein parameters estimated experimentally all fall into the black box in the incoherent, transport-limited regime. (b–f) Acceptor populations dynamics simulated with HEOM for different values of coupling to the thermal environments. The dashed line corresponds to one period of unitary dynamics between the donor and vibrationally excited acceptor states. These calculations use $V_{vib} = 0.788$ cm^{-1}, $\gamma_{elec} = 50$ cm^{-1}, and $E_d - E_a = 350$ cm^{-1}.

DOI: 10.1021/acs.jpclett.8b00844
J. Phys. Chem. Lett. 2018, 9, 2665–2670

IIIA). We find that $k_{a\leftarrow d}$ is maximized when the rate of vibrational relaxation is comparable to the vibronic coupling ($\Gamma_{vib} \approx 1$) and there are minimal thermal fluctuations from the low-frequency vibrational modes ($\Lambda_{vib} \approx 0$). The corresponding total acceptor population dynamics show a rapid rise, followed by minimal subsequent oscillations (solid line, Figure 2d). The initial rise in acceptor population dynamics is similar to the dynamics expected between the donor and vibrationally excited acceptor in the absence of any thermal environments (dashed line, Figure 2d). This similarity suggests that these dynamics correspond to an early time delocalization between the donor and acceptor pigments supported by the resonant vibration.

We quantify the extent of early time delocalization between the donor and vibrationally excited acceptor states by integrating the absolute value of the corresponding off-diagonal element of the vibronic Redfield density matrix (ρ_{coh}= $|A,1_e\rangle\langle D,0_g|$) over one half period of the acceptor population oscillation (T_{coh}), shown as a colored region in Figure 3a.

$$M_{coh} = \frac{\int_0^{T_{coh}} |\rho_{coh}(t)|\, dt}{\int_0^{T_{coh}} |\rho_{coh}^{\Lambda=0,\Gamma=0}(t)|\, dt} \quad (5)$$

The extent of coherence decreases as a function of increasing Γ_{vib}, leading to incoherent transport when Γ_{vib} = 10, even if coupling to the electronic environment remains weak (purple circles, right axis, Figure 3b). The same transition to an incoherent mechanism occurs more rapidly with increasing magnitude of thermal fluctuations driven by the low-frequency vibrations (Λ_{elec}), where we find incoherent transport begins by $\Lambda_{elec} \approx 1$. The transition from coherent ($M_{coh} > 0.8$) to incoherent ($M_{coh} < 0.2$) dynamics is reflected in the early time behavior of the acceptor population (Figure 2b,d,e): For coherent dynamics, the initial donor excitation performs ballistic transport, resulting in at least one large sinusoidal oscillation of acceptor population; for incoherent dynamics, the donor excitation performs incoherent hopping transport, resulting in a slower exponential rise.

In our model of the vibronic heterodimer, the energy gap between the electronic donor and acceptor states is large enough ($\Delta E \approx \Omega_{vib} \gg V,\lambda_{elec}$) that transport following an initial donor excitation has only two components (Supporting Information section ID): vibronic transport between nearly degenerate donor and acceptor states (e.g., $|D,0_g\rangle \rightarrow |A,1_e\rangle$) and vibrational relaxation (e.g., $|A,1_e\rangle \rightarrow |A,0_e\rangle$). We decompose vibronic dynamics into these two fundamental processes by fitting rate matrix parameters to Redfield population curves for vibrational states up to $\nu_{e/g}$ = 2, as described in Supporting Information section IIIC. Figure 3b shows the best-fit vibronic transport rate (k_{trans}, orange lines, left axis), vibrational relaxation rate (k_{relax}, green lines, left axis), and the overall donor-to-acceptor rate ($k_{a\leftarrow d}$, black line, left axis) when thermal fluctuations are small (Λ_{elec} = 0.01). When k_{trans} (k_{relax}) is the smaller of the two best-fit rates and no more that 0.04 larger than $k_{a\leftarrow d}$, we consider the dynamics to be transport (relaxation) limited. When the relaxation rate is slow compared with the vibronic coupling ($\Gamma_{vib} \ll 1$), vibrational relaxation is the rate-limiting step to achieve maximal excitation population on the acceptor. Relaxation-limited vibronic dynamics explains the two time scales observed in the acceptor population when $\Gamma_{vib} \ll 1$ (Figure 2b,c): Excitation transports rapidly between the donor and vibrationally excited acceptor states but reaches the ground vibrational state of the acceptor ($|A,0_e\rangle$) only after the slower process of vibrational relaxation. In the opposite extreme, when the relaxation rate is very fast ($\Gamma_{vib} \gg 1$), vibronic transport is rate-limiting. In the transport-limited regime, the total acceptor population (Figure 2e,f) shows a single time scale representative of the rate of vibronic transport from the donor to the acceptor, which is followed by rapid vibrational relaxation.

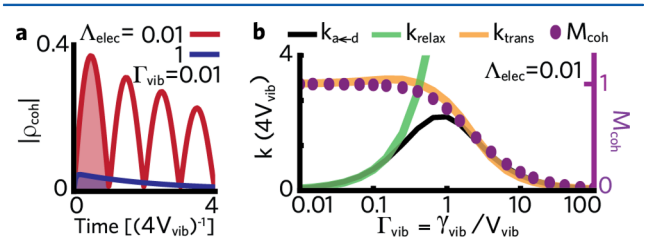

Figure 3. (a) $|\rho_{coh}|$ calculated by vibronic Redfield as a function of time. (b) Overall rate from the donor to acceptor is superimposed with the best-fit vibronic transport (k_{trans}) and relaxation (k_{relax}) rates as a function of Γ_{vib} when Λ_{elec} = 0.01. Other parameters are the same as in Figure 2.

We describe the vibronic transport mechanism by the extent of coherence (red and blue solid lines, Figure 2a) and the potential for a rate-limiting step (green and orange dashed lines, Figure 2a). Vibronic transport in phycobiliproteins tends to be well approximated by an effective dimer model because of the relatively large distances between most bilins.[2,5] Surprisingly, using the parameters extracted from spectroscopic measurements, all three phycobiliproteins previously assigned to show coherent vibronic transport[3,20,21] (Supporting Information section 4) fall well into the incoherent regime (black box, Figure 2a). This conclusion is robust to substantial variations in Hamiltonian parameters that might vary the ratio of λ_{elec} to V_{vib}. Furthermore, this is consistent with a recent reanalysis of a phycobiliprotein, PC645, which revealed, using HEOM calculations, an incoherent vibronic transport mechanism.[5] Whereas the mechanistic map presented here assumes a rapidly relaxing (i.e., Markovian) thermal environment, the addition of non-Markovian modes would only allow for coherence on time scales that are short compared with the relaxation time scale ($1/\gamma_{elec}$). Detailed simulations of bilin motion in PC645 suggest that a large inertial component of nuclear reorganization occurs on a time scale of ∼20 fs, whereas vibronic transport in both simulation and experiment is found to occur on time scales of >500 fs, consistent with a Markovian approximation.[5] These results provide strong evidence that vibronic transport in phycobiliproteins is incoherent. Whereas the current model reproduces long-lived oscillations in 2D electronic spectroscopy, further work is needed to identify potential spectroscopic signatures of the mechanistic regimes outlined here.

Does the incoherent nature of vibronic transport in phycobiliproteins point toward inefficiency or an unexplained design principle? Up to this point we have considered the high-frequency vibration to be perfectly resonant with the energy gap between pigments. As a result, we always see the overall donor-to-acceptor rate ($k_{a\leftarrow d}$) decrease with increasing magnitude of thermal fluctuations (Λ_{elec}). In the presence of an energy gap between the donor and vibrationally excited acceptor ($\Sigma_{vib} \neq 0$), however, increasing the magnitude of thermal fluctuations can increase the fraction of time that the two states spend near resonance, thereby enhancing the overall

DOI: 10.1021/acs.jpclett.8b00844
J. Phys. Chem. Lett. 2018, 9, 2665−2670

donor-to-acceptor rate (red/blue line, Figure 4a), analogous to the environmentally assisted quantum transport (ENAQT) mechanism previously observed in electronic transport.[16,17,36,37] In practice, molecular aggregates, photosynthetic pigment protein complexes among them, have an ensemble of conformations with slightly different pigment excitation energies leading to energetic disorder. For phycobiliproteins, energetic disorder is expected to have a standard deviations of at least $10V_{vib}$ (gray line, Figure 4a), as explained in Supporting Information section IVD. If we calculate the distribution of the overall donor-to-acceptor rate ($k_{a\leftarrow d}$) in a representative disordered ensemble (Supporting Information section IIID), shown in Figure 4b, then we find that 50% of dimers have a rate <0.1 when $\Lambda_{elec} = 0.01$, compared with only 4% of dimers when $\Lambda_{elec} = 1$. Under physiological conditions, absorbed excitation must be successfully transferred through most antenna complexes, not merely the set of resonant complexes. In this context, the incoherent vibronic transport mechanism of phycobiliproteins is, in fact, better for functional light-harvesting antennae. This points to a basic design principle for vibronic transport: Incoherent mechanisms are more robust to disorder and therefore are expected to be more efficient when the magnitude of disorder exceeds the vibronic coupling.

The advantage of incoherent vibronic transport in the presence of disorder highlights an important requirement for engineering new materials that use a coherent vibronic mechanism: There must be limited energetic disorder relative to the vibronic coupling. Photosynthetic pigment protein complexes greatly reduce energetic disorder compared with most synthetic aggregates by reproducibly folding with specific pigment positions and orientations, but still we find that at least in some cases disorder can exceed the vibronic coupling. Therefore, we suggest that one of the key challenges for engineering materials to enable coherent vibronic transport is to develop new synthetic structures that dramatically reduce energetic disorder. Finally, our results also suggest that a re-evaluation of the role of coherence in vibronic transport for other families of photosynthetic pigment protein complexes may be appropriate. The mechanistic map developed here provides a simple rule-of-thumb for determining the extent of coherence in a vibronic heterodimer. Previous work in electronic transport has shown that the transition from coherent to incoherent regimes, used to define the domains of pigments appropriate for generalized Förster theory,[18,19] follows similar rules of thumb as the electronic dimer. In the case of the Fenna−Matthews−Olson (FMO) complex, for example, the Hamiltonian parameters[11] give $\Lambda_{elec} > 3$, which suggests that vibronic transport occurs via an incoherent mechanism, even in the presence of motional narrowing[38] arising from exciton delocalization. This conclusion is consistent with the recent reinterpretation of the 2D optical spectra.[13] Thus we expect that our current results provide a foundation for understanding the mechanism of transport in larger photosynthetic aggregates where coherent vibronic transport has been proposed.[9−11]

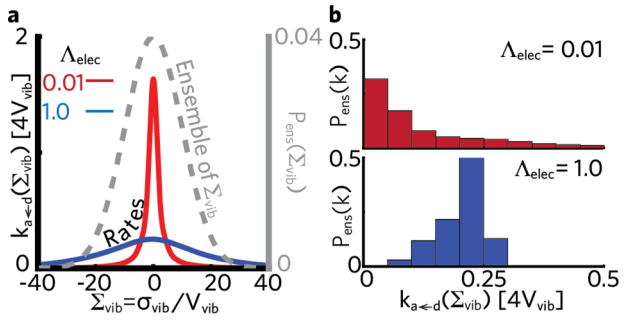

Figure 4. (a) Rate of equilibration (left axis) when $\Gamma_{vib} = 1$ and $\Lambda_{elec} = 0.01$ (red line) or 1 (blue line) is plotted as a function of the energetic detuning between the donor and vibrationally excited acceptor state (Σ_{vib}). A representative ensemble of Σ_{vib} has a standard deviation of 10 (gray dashed line, right axis). (b) Probability of a given rate of equilibration is plotted for $\Lambda_{elec} = 0.01$ (top panel) and $\Lambda_{elec} = 1$ (bottom panel) assuming a Gaussian ensemble of Σ_{vib} with standard deviation of 10. Other parameters are the same as in Figure 2.

■ ASSOCIATED CONTENT

Supporting Information

The Supporting Information is available free of charge on the ACS Publications website at DOI: 10.1021/acs.jpclett.8b00844.

Section I: Vibronic dimer Hamiltonian and connection between electronic and vibronic basis. Section II: Computational details of HEOM simulations, bounds on the high-temperature approximation for underdamped Brownian oscillators, and computational details of vibronic Redfield simulations. Section III: Description of extracting total donor-to-acceptor transport rate ($k_{a\leftarrow d}$), comparison of HEOM and vibronic Redfield simulations in Markovian and less Markovian regimes, description of determining the effective transport and relaxation rates, and description of treating disorder ensembles of vibronic dimers. Section IV: Parameter extraction for effective dimer models of photosynthetic pigment protein complexes. (PDF)

■ AUTHOR INFORMATION

Corresponding Author

*E-mail: doranbennett@g.harvard.edu.

ORCID

Doran I. G. Bennett: 0000-0001-8322-7371

Alán Aspuru-Guzik: 0000-0002-8277-4434

Notes

The authors declare no competing financial interest.

■ ACKNOWLEDGMENTS

We acknowledge the Center for Excitonics, an Energy Frontier Research Center funded by the U.S. Department of Energy, Office of Science and Office of Basic Energy Sciences, under award number DE-SC0001088. D.I.G.B., A.A.-G., P.M., and R.v.G. acknowledge CIFAR, the Canadian Institute for Advanced Research, for support through the Bio-Inspired Solar Energy program. D.I.G.B. and A.A.-G. acknowledge the John Templeton Foundation (grant number 60469). P.M. acknowledges the Czech Science Foundation (GACR) grant no. 17-22160S. We thank Nvidia for support via the Harvard CUDA Center of Excellence. This research used computational time on the Odyssey cluster, supported by the FAS Division of Science, Research Computing Group at Harvard University.

■ REFERENCES

(1) Scholes, G. D.; Fleming, G. R.; Chen, L. X.; Aspuru-Guzik, A.; Buchleitner, A.; Coker, D. F.; Engel, G. S.; Van Grondelle, R.; Ishizaki, A.; Jonas, D. M.; et al. Using Coherence to Enhance Function in Chemical and Biophysical Systems. *Nature* **2017**, *543*, 647.

DOI: 10.1021/acs.jpclett.8b00844
J. Phys. Chem. Lett. 2018, 9, 2665−2670

(2) O'Reilly, E. J.; Olaya-Castro, A. Non-Classicality of the Molecular Vibrations Assisting Exciton Energy Transfer at Room Temperature. *Nat. Commun.* **2014**, *5*, 3012.
(3) Dean, J. C.; Mirkovic, T.; Toa, Z. S.; Oblinsky, D. G.; Scholes, G. D. Vibronic Enhancement of Algae Light Harvesting. *Chem.* **2016**, *1*, 858−872.
(4) Killoran, N.; Huelga, S. F.; Plenio, M. B. Enhancing Light-Harvesting Power with Coherent Vibrational Interactions: A Quantum Heat Engine Picture. *J. Chem. Phys.* **2015**, *143*, 155102.
(5) Blau, S. M.; Bennett, D. I.; Kreisbeck, C.; Scholes, G. D.; Aspuru-Guzik, A. Local protein solvation drives direct down-conversion in phycobiliprotein PC645 via incoherent vibronic transport. *Proc. Natl. Acad. Sci. U. S. A.* **2018**, *115*, E3342.
(6) Schreiber, A.; Cassemiro, K.; Potoček, V.; Gábris, A.; Jex, I.; Silberhorn, C. Decoherence and disorder in quantum walks: from ballistic spread to localization. *Phys. Rev. Lett.* **2011**, *106*, 180403.
(7) Akselrod, G. M.; Deotare, P. B.; Thompson, N. J.; Lee, J.; Tisdale, W. A.; Baldo, M. A.; Menon, V. M.; Bulović, V. Visualization of exciton transport in ordered and disordered molecular solids. *Nat. Commun.* **2014**, *5*, 3646.
(8) Chin, A.; Prior, J.; Rosenbach, R.; Caycedo-Soler, F.; Huelga, S.; Plenio, M. The Role of Non-Equilibrium Vibrational Structures in Electronic Coherence and Recoherence in Pigment-Protein Complexes. *Nat. Phys.* **2013**, *9*, 113−118.
(9) Romero, E.; Augulis, R.; Novoderezhkin, V. I.; Ferretti, M.; Thieme, J.; Zigmantas, D.; Van Grondelle, R. Quantum Coherence in Photosynthesis for Efficient Solar-Energy Conversion. *Nat. Phys.* **2014**, *10*, 676−682.
(10) Fuller, F. D.; Pan, J.; Gelzinis, A.; Butkus, V.; Senlik, S. S.; Wilcox, D. E.; Yocum, C. F.; Valkunas, L.; Abramavicius, D.; Ogilvie, J. P. Vibronic Coherence in Oxygenic Photosynthesis. *Nat. Chem.* **2014**, *6*, 706−711.
(11) Nalbach, P.; Mujica-Martinez, C.; Thorwart, M. Vibronically Coherent Speed-Up of the Excitation Energy Transfer in the Fenna-Matthews-Olson Complex. *Phys. Rev. E* **2015**, *91*, 022706.
(12) Fujihashi, Y.; Fleming, G. R.; Ishizaki, A. Impact of Environmentally Induced Fluctuations on Quantum Mechanically Mixed Electronic and Vibrational Pigment States in Photosynthetic Energy Transfer and 2D Electronic Spectra. *J. Chem. Phys.* **2015**, *142*, 212403.
(13) Duan, H.-G.; Prokhorenko, V. I.; Cogdell, R. J.; Ashraf, K.; Stevens, A. L.; Thorwart, M.; Miller, R. J. D. Nature Does Not Rely on Long-Lived Electronic Quantum Coherence for Photosynthetic Energy Transfer. *Proc. Natl. Acad. Sci. U. S. A.* **2017**, *114*, 8493−8498.
(14) Wilkins, D. M.; Dattani, N. S. Why quantum coherence is not important in the Fenna−Matthews−Olsen complex. *J. Chem. Theory Comput.* **2015**, *11*, 3411−3419.
(15) Dijkstra, A. G.; Wang, C.; Cao, J.; Fleming, G. R. Coherent Exciton Dynamics in the Presence of Underdamped Vibrations. *J. Phys. Chem. Lett.* **2015**, *6*, 627−632.
(16) Ishizaki, A.; Fleming, G. R. Unified Treatment of Quantum Coherent and Incoherent Hopping Dynamics in Electronic Energy Transfer: Reduced Hierarchy Equation Approach. *J. Chem. Phys.* **2009**, *130*, 234111.
(17) Rebentrost, P.; Mohseni, M.; Kassal, I.; Lloyd, S.; Aspuru-Guzik, A. Environment-Assisted Quantum Transport. *New J. Phys.* **2009**, *11*, 033003.
(18) Novoderezhkin, V.; Marin, A.; van Grondelle, R. Intra- and Inter-Monomeric Transfers in the Light Harvesting LHCII Complex: the Redfield-Forster Picture. *Phys. Chem. Chem. Phys.* **2011**, *13*, 17093−17103.
(19) Raszewski, G.; Renger, T. Light Harvesting in Photosystem II Core Complexes Is Limited by the Transfer to the Trap: Can the Core Complex Turn into a Photoprotective Mode? *J. Am. Chem. Soc.* **2008**, *130*, 4431−4446.
(20) Womick, J. M.; Moran, A. M. Vibronic Enhancement of Exciton Sizes and Energy Transport in Photosynthetic Complexes. *J. Phys. Chem. B* **2011**, *115*, 1347−1356.
(21) Kolli, A.; O'Reilly, E. J.; Scholes, G. D.; Olaya-Castro, A. The Fundamental Role of Quantized Vibrations in Coherent Light Harvesting by Cryptophyte Algae. *J. Chem. Phys.* **2012**, *137*, 174109.
(22) Garg, A.; Onuchic, J. N.; Ambegaokar, V. Effect of friction on electron transfer in biomolecules. *J. Chem. Phys.* **1985**, *83*, 4491−4503.
(23) Warshel, A.; Parson, W. W. Computer simulations of electron-transfer reactions in solution and in photosynthetic reaction centers. *Annu. Rev. Phys. Chem.* **1991**, *42*, 279−309.
(24) Fleming, G. R.; Cho, M. Chromophore-solvent dynamics. *Annu. Rev. Phys. Chem.* **1996**, *47*, 109−134.
(25) Jordanides, X. J.; Lang, M. J.; Song, X.; Fleming, G. R. Solvation dynamics in protein environments studied by photon echo spectroscopy. *J. Phys. Chem. B* **1999**, *103*, 7995−8005.
(26) Gryliuk, G.; Rätsep, M.; Hildebrandt, S.; Irrgang, K.-D.; Eckert, H.-J.; Pieper, J. Excitation energy transfer and electron-vibrational coupling in phycobiliproteins of the cyanobacterium Acaryochloris marina investigated by site-selective spectroscopy. *Biochim. Biophys. Acta, Bioenerg.* **2014**, *1837*, 1490−1499.
(27) Viani, L.; Corbella, M.; Curutchet, C.; O'Reilly, E. J.; Olaya-Castro, A.; Mennucci, B. Molecular basis of the exciton−phonon interactions in the PE545 light-harvesting complex. *Phys. Chem. Chem. Phys.* **2014**, *16*, 16302−16311.
(28) Aghtar, M.; Kleinekathöfer, U. Environmental coupling and population dynamics in the PE545 light-harvesting complex. *J. Lumin.* **2016**, *169*, 406−409.
(29) Chenu, A.; Christensson, N.; Kauffmann, H. F.; Mančal, T. Enhancement of vibronic and ground-state vibrational coherences in 2D spectra of photosynthetic complexes. *Sci. Rep.* **2013**, *3*, 2029.
(30) Iles-Smith, J.; Dijkstra, A. G.; Lambert, N.; Nazir, A. Energy transfer in structured and unstructured environments: Master equations beyond the Born-Markov approximations. *J. Chem. Phys.* **2016**, *144*, 044110.
(31) Malý, P.; Somsen, O. J.; Novoderezhkin, V. I.; Mančal, T.; van Grondelle, R. The Role of Resonant Vibrations in Electronic Energy Transfer. *ChemPhysChem* **2016**, *17*, 1356−1368.
(32) Tiwari, V.; Peters, W. K.; Jonas, D. M. Electronic energy transfer through non-adiabatic vibrational-electronic resonance. I. Theory for a dimer. *J. Chem. Phys.* **2017**, *147*, 154308.
(33) Tanimura, Y.; Kubo, R. Time Evolution of a Quantum System in Contact with a Nearly Gaussian-Markoffian Noise Bath. *J. Phys. Soc. Jpn.* **1989**, *58*, 101−114.
(34) Tanimura, Y. Reduced Hierarchy Equations of Motion Approach with Drude Plus Brownian Spectral Distribution: Probing Electron Transfer Processes by Means of Two-Dimensional Correlation Spectroscopy. *J. Chem. Phys.* **2012**, *137*, 22A550.
(35) Kreisbeck, C.; Kramer, T.; Aspuru-Guzik, A. Scalable High-Performance Algorithm for the Simulation of Exciton Dynamics. Application to the Light-Harvesting Complex II in the Presence of Resonant Vibrational Modes. *J. Chem. Theory Comput.* **2014**, *10*, 4045−4054.
(36) Sisto, A.; Stross, C.; van der Kamp, M. W.; O'Connor, M.; McIntosh-Smith, S.; Johnson, G. T.; Hohenstein, E. G.; Manby, F. R.; Glowacki, D. R.; Martinez, T. J. Atomistic non-adiabatic dynamics of the LH2 complex with a GPU-accelerated ab initio exciton model. *Phys. Chem. Chem. Phys.* **2017**, *19*, 14924−14936.
(37) van der Vegte, C.; Prajapati, J.; Kleinekathöfer, U.; Knoester, J.; Jansen, T. Atomistic modeling of two-dimensional electronic spectra and excited-state dynamics for a light harvesting 2 complex. *J. Phys. Chem. B* **2015**, *119*, 1302−1313.
(38) Mukamel, S. *Principles of Nonlinear Optical Spectroscopy*; Oxford University Press on Demand, 1999.

DOI: 10.1021/acs.jpclett.8b00844
J. Phys. Chem. Lett. 2018, 9, 2665−2670